Journal of Scientific & Industrial Research
Vol. 82, June 2023, pp. 642-651
DOI: 10.56042/jsir.v82i06.1971

Efficient Restoration of Magnetic Resonance Images Corrupted with Impulse Noise using Spatial Constraints based Fuzzy Decision Filter

Priyank Saxena* & R Sukesh Kumar
Electronics & Communication Engineering Department, Birla Institute of Technology, Mesra, Ranchi, Jharkhand 835 215, India

Received 04 September 2021; revised 28 May 2023; accepted 29 May 2023

Magnetic Resonance (MR) images are subject to unavoidable noises during the data acquisition due to imperfections of device components and trade-offs in the scan parameters. The study proposes a two-step Fuzzy Decision-Based Filter (FDBF) as a post-reconstruction technique to mitigate random valued impulse noise from MR images. The FDBF employs a Spatial Fuzzy C-means (SFCM) clustering for detection and an Intensity Based Fuzzy Estimation (IBFE) technique for restoration. Firstly, SFCM integrates the spatial relation of the adjacent pixels into the membership function to form three separate clusters. The IBFE technique leaves the noise-free cluster unaltered while restoring the remaining in the second step. IBFE incorporates neighbor pixel correlation to restore the corrupted pixel leading to edge preservation. To assess the efficacy of the intended method both the quality metrics and the observed quality of the restored images are considered. The suggested detection strategy using SFCM performs very well, up to a 93% corruption level with zero false and miss detection rates even when there is intensity in homogeneity among pixels. Compared to other existing filtering techniques, the proposed two-step restoration method significantly improves the perceived image quality and other image quality metrics of the restored image without obliterating more intricate details and finer structures. FDBF considers the spatial information of the nearby pixels during the detection and restoration processes, which is essential for MR image restoration.

Keywords: Decision-based filter, Edge preservation, Image restoration, Intensity-based fuzzy estimation, Spatial fuzzy C-means clustering

Introduction

MR (Magnetic Resonance) images are widely used to examine the anatomy and physiology of the human being. MR images are used to examine different soft tissues because of their high spatial resolution and high contrast in contrast to the other imaging modalities.[1] These images often get corrupted with noise, artefacts, etc., during collection due to hardware imperfection and other reasons. The noise in MR images significantly impacts the diagnosis and the result of various post-processing techniques such as segmentation and registration applied to image data.[2] MR images are frequently distorted during acquisition, recording, and transmission with unavoidable noises because of using low-quality sensors.[3] Impulse noise has the characteristic of affecting a percentage of the image's pixels only and can be categorized as bipolar or unipolar. The textural and edge details of a Gray-scale image (8-bit) are degraded because of bi-polar impulse noise corrupting pixels with the extreme (255) or least (0) values present. In contrast, the intensity values of the pixels corrupted with Random Valued Impulse Noise (RVIN) can take any value between the minimum and maximum.

The major goal of restoring an MR image is to correct the intensity inhomogeneity among the pixels introduced by the bias field degradation while preserving the edge information and other clinically relevant features. The post-processing filtering methods have been extensively used because they remove noise from MR images allowing a smaller acquisition period.[4]

The noise reduction strategies can be broadly divided into spatial and temporal domains. The proposed study focuses on the spatial domain which can be further categorized as linear and non-linear filtering.[5] Linear filtering causes the blurring of edges in an image while removing RVIN. Conventional Median Filtering[6] (CMF) is quite famous for RVIN removal among the many nonlinear filtering methods. CMF performs well at low corruption levels but fails to preserve the edge information of an image at high levels of corruption. By extending the notions of CMF, several changes to CMF have been proposed. Several amendments to CMF have been recommended by just extending the notions of CMF.[7–9] The chosen

*Author for Correspondence
E-mail: priyanksaxena@bitmesra.ac.in

pixels in each operating window undergo multiplication by the specified weights in the Weighted Median Filter[7] (WMF) and Centre Weighted Median Filter[8] (CWMF) causing alteration of the pixels without noise hence affecting the denoising performance. Modifying noise-free pixels is the primary reason for their failure when applied to the entire image. The adapted window size is utilized in Adaptive Median Filter[9] (AMF) but resulted in exceptionally high computation time at high levels of corruption.

To address the above-listed shortcomings, Decision-Based (DB) or switching strategy-based filters have been suggested. The major goal of DB filters is to separate the noisy pixels and restore them without modifying the normal ones. The efficacy of the DB filters lies in detecting impulses to achieve accurate restoration. The impulse detection stage of most of the DB methods available in the literature can be categorized mainly based on thresh holding, histogram, and clustering detection. Some well-known decision-based filtering techniques are the Switching Median (SM) filter.[10–23] Early-developed SM filters have shown significant improvement over the conventional ones, but the impulse detector based on the median failed to interpret impulses correctly and removed thin lines instead of impulses. Among the different SM filters, Signal-Dependent Rank-Ordered Mean[19] (SD-ROM), and Noise Adaptive Soft-Switching Median[20] (NASM) impulse detectors were found to be efficient but increase the computational complexity at the high percentage of noise density. A Boundary Discriminative Noise Detector[21] (BDND) is the popular switching median filter. However, the size of the filtering kernel is subjected to some stringent conditions without considering the noise density. Improved Boundary Discriminative Noise Detector[22] (IBDND) overcomes the drawback of the BDND. Decision-based filters using local information exhibit considerable performance improvement. Improved Switching Vector Median Filter[23] (ISVMF) provides better results to some extent due to the consideration of the local threshold when tested on Lena Image.

Several decision-based nonlinear methods using fuzzy reasoning have been proposed in the literature and found effective in impulse noise detection and removal.[24–31] Fuzzy-based methods perform well in handling the inherent vagueness and ambiguity in the local information when restoration of corrupted images is required without abolishing the image details. A two-step Fuzzy-Impulse-Noise-Detection and Reduction Method[25] (FIDRM) employs a fuzzy-logic approach to detect and remove impulse noise of all kinds. A Fuzzy Based Decision Algorithm[26] (FBDA) performs impulse detection by computing the intensity variation of each pixel concerning the noisy pixel (center pixel). It assigns the membership value to each pixel based on the maximum intensity variation in a selected window. FBDA uses a median filter for restoration. Filters employing rule-based fuzzy adaptive median, adaptive fuzzy, fuzzy rules-based impulse detection, and similarly valued neighbor criterion give good results but at high computing costs.[27,29–31]

Recent advancements in the field of Artificial Learning (AI) have attracted researchers to use them for denoising images. Recently published studies included the Convolutional Neural Networks (CNN) for RVIN removal from medical images.[32–35]

From the above discussion, it can be concluded that the primary concern of the impulse detection step is intensity in homogeneity among the pixels of an MR image created by the RVIN. The summary of related work with the research gap is as follows:

- The issue with CNN-based methods is that they demand significant computational resources to train CNN from scratch. For proper model parameter tweaking, it takes time, and a huge, annotated database is required. Transfer learning may be the answer, although depending on the kind of pre-trained network being utilized, the image size may need to be reduced (or downsized). The resolution and texture information will be negatively impacted compromising the diagnostic quality of the image. Though, generative models have demonstrated promising results.
- Most of the DB methods look exclusively for significant outliers and fail to detect tiny impulses (pixels with slight intensity differences from their original value), creating a grainy appearance.
- The detection stage becomes even more important if the noise is present because of inadequate contrast in medical images.
- In most of the DB methods, restoration of the corrupted pixel is executed by fixing it with the median value or its modifications. These methods do not consider the neighbor pixel

correlation. Therefore, they usually result in blurring image details due to averaging even at mild noise density.

The proposed study does not require any annotated dataset and high computation compared to CNN-based methods. The significant contributions of this study are as follows.

- It is considered that the intensities of low and high-impulse noises are unequal in density.
- The spatial correlation of the adjoining pixels is exploited during impulse detection using SFCM and restoration using IBFE.
- SFCM has been used for impulse detection distinguishing the pixels with or without noise by partitioning them into three clusters and need not require any training or optimizing parameters.
- The proposed IBFE technique incorporates neighbor pixel correlation to restore the corrupted pixel, preserving more edge details. Membership values are assigned for distinct pixel intensities in proportion to the noise level of a pixel. The estimated restoration value of the pixel with noise is assessed by utilizing the fuzzy membership function to allocate weights to the neighbors in proportion to their intensity values.
- The FDBF's efficacy is assessed as per the quality metrics and observed quality of the restored image. FDBF delivers favorably against the other existing methods at optimum computing cost.

Materials and Methods

This study aims to identify and eliminate RVIN of high density from an MR Image without sacrificing clinically significant information. The proposed two-step FBDF model uses SFCM for identification and IBFE for the restoration of the pixels affected by RVIN.

Impulse Noise Model

The biggest challenge is correctly identifying the pixels of an image as impulses. Therefore, pixels with significant intensity differences from their neighbouring pixels are identified as impulses. For a pixel location(i,j), let $G_{i,j}$ represents the pixel intensity of the original image I and $G'_{i,j}$ represents the gray level of noisy images and $[G_{min} = 0, G_{max} = 255]$ represents the range of pixel intensity levels for a monochrome image. An image corrupted by RVIN with probability p can be defined as per the following:

$$G'_{i,j} = \begin{Bmatrix} N_{i,j}\ with\ probability\ p \\ G_{i,j}\ with\ probability\ 1-p \end{Bmatrix}$$

where, $N_{i,j}$ represents the random number in the dynamic range between G_{min} and G_{max}.

Impulse Detection using Spatial FCM

The efficiency of the image restoration technique largely rests on the correct identification of the impulses. Fuzzy C-means (FCM) is the most widely used clustering technique for the classification of image data. In FCM, the data sample is assigned a membership value in the range of 0 to 1 depending on how similar it is to the cluster center.[36] FCM's primary goal is to iteratively lessen the following cost function to partition an image with *N* number of pixels into *c*-clusters given by Eq. (1).

$$J = \sum_{j=1}^{N}\sum_{i=1}^{c} {u_{ij}}^{m} \left\|x_j - v_i\right\|^2 \quad \ldots (1)$$

where,

u_{ij}: degree of membership of x_i in the cluster i;

x_j: j^{th} data of d-dimensional measured data;

$\left\|x_j - v_i\right\|^2$: Euclidean distance between j^{th} data and i^{th} cluster center;

m - fuzziness index, considered as m = 2 in this study;

The Eqs (2) & (3) update the membership functions and cluster centers.

$$u_{ij} = \frac{1}{\sum_{k=1}^{c}\left(\frac{\left\|x_j - v_i\right\|}{\left\|x_j - v_k\right\|}\right)^{2/(m-1)}} \quad \ldots (2)$$

$$v_i = \frac{\sum_{j=1}^{N} {u_{ij}}^{m} x_j}{\sum_{j=1}^{N} {u_{ij}}^{m}} \quad \ldots (3)$$

On convergence, defuzzification is performed to find the clusters. Conventional FCM fails to perform well in non-uniform intensity distribution and noise; therefore, modification to FCM with spatial information is proposed.[37] In SFCM, every iteration implies two stages in the clustering practice. The first stage is similar to the traditional FCM. A spatial function mentioned in Eq. (4) is described in the second stage as the total of all membership values in

the spatial domain in the pixel's immediate vicinity.

$$h_{ij} = \sum_{k \in NB(x_j)} u_{ik} \quad \ldots (4)$$

where, $NB(x_j)$ represents a window of size 5×5 centered on a pixel x_j in the spatial domain. In Eq. (5), h_{ij} represents the likelihood that pixel x_j belongs to i^{th} cluster similar to the membership function. If most of a pixel's neighborhood is comprised of other pixels from the same clusters, h_{ij} of that pixel is likely to be big.

$$u'_{ij} = \frac{{u_{ij}}^a {h_{ij}}^b}{\sum_1^c {u_{kj}}^a {h_{kj}}^b} \quad \ldots (5)$$

where, a and b are variables that regulate the respective weights of both functions, and c specifies the count of clusters. In a homogeneous area, the clustering conclusion holds, and the spatial functions support the initial membership. This formula, however, reduces the weighting of a noisy cluster by the labels of its neighbouring clusters for a noisy pixel. This method significantly lessens the impact of noise and biases the algorithm in favour of homogeneous grouping.

The FCM iteration gains a new membership that includes the spatial function. When the largest difference between two cluster centers at two following iterations is less than a threshold (= 0.02), the iteration is over. Each pixel is assigned to the cluster with the highest membership following convergence using defuzzification.

SFCM divides the neighbourhood of the center pixel unsupervised using a kernel of size 5×5, into three different clusters of low intensity, high intensity, and noise-free clusters, respectively. After forming clusters, let the maximum value of each cluster be L_1, L_2, and L_3, respectively. The extreme intensity level from each cluster is chosen and arranged in ascending order ($L_1 < L_2 < L_3$) to separate the boundary of each cluster. The following assumption is used to determine whether the center pixel $P\,(i,j)$ is noisy or noise-free.

$$P\,(i,j) = \begin{cases} \text{Low-intensity cluster (LIC): if } P(i,j) < L1. \\ \text{Noise-free cluster (NFC): if } L1 < P\,(i,j) \leq L2. \\ \text{High-intensity cluster (HIC): if } L2 < P\,(i,j) \leq L3. \end{cases}$$

Image Restoration using Intensity Fuzzy Estimation

The restoration of the contaminated pixel by the median value of the operating kernel is not carried out by the intended method. Restoration of the median value can produce good results only when the considered pixels are somehow similar to each other. However, there are sufficient possibilities that the neighbourhood will be extremely dissimilar for images degraded with high-density RVIN. The restoration of pixels corrupted with RVIN is performed using an intensity-based fuzzy estimation. Membership values are assigned for various pixel intensities based on the amount of noise in each pixel.

By utilizing the fuzzy membership function to assign weights to the neighbours based on their intensity values, it is possible to get the estimated restoration value of the center pixel. These weights are being considered as the similarity measure in which the pixels are similar with their predefined neighbours and hence will contribute accordingly. Therefore, the fuzzy value of that pixel will show how much noise is there in the center pixel under scrutiny. The fuzzy set used is depicted in Fig. 1 and is described by the fuzzy membership function below. For best results, the fuzzy input variable is set to the local information (pixel intensity).

$$F\,(i,j) = \begin{cases} \dfrac{P\,(i,j)}{l_1} \; 0 \leq P(i,j) < L_1 \\ 1 \;\; L_1 \leq P(i,j) < L_2 \\ \dfrac{P\,(i,j) - L_3}{L_2 - L_3} \; L_2 \leq P(i,j) < L_3 \end{cases}$$

Finally, the estimated restoration term $R\,(i,j)$ for the corrupted pixel $X\,(i,j)$ in an image, **I** can be computed based on the fuzzy weights assigned to the 24 neighbors in a 5×5 window as per their pixel intensity as defined by Eq. (6).

$$R(i,j) = \big(1 - F\,(i,j)\big) \frac{\sum_{k=2}^{2} \sum_{i=2}^{2} I\,(i+k,j+l) F(i+k,j+l)}{\sum_{k=2}^{2} \sum_{i=2}^{2} F(i+k,j+l)} + F(i,j).I\,(i,j) \quad \ldots (6)$$

To estimate the restored value, the fuzzy value of the corrupted pixel, indicates the amount of noise

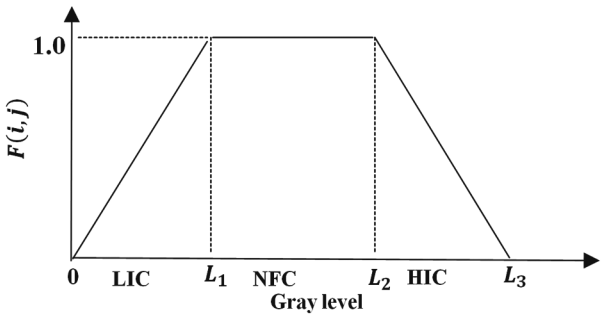

Fig.1 — Fuzzy membership function

present in the pixel. The fuzzy weight assigned to the center pixel will be one if it is a member of the noise-free cluster. Because of this, the predicted restoration value is equal to the value of the original pixel. The fuzzy weights are instead assigned based on the fuzzy membership function depending on the intensity value of the centre pixel whether it is a member of the noisy cluster or not. Edge preservation is achieved by computing the estimated restoration value for the noisy pixel based on its neighbourhood correlation.

Results and Discussion

Based on experiments conducted on several MR test images, the performance of the proposed FDBF approach is assessed. The test images have additive RVIN contamination with a density ranging from 10% to 90%. The following image quality assessment measures have been used to gauge how well FDBF restores MR images.[38]

Image Quality Assessment Metrics

Mean-Square Error (MSE)

A noise-free monochromatic image P of size m × n and its noisy approximation P' are both used to define MSE in Eq. (7).

$$MSE = \frac{1}{mn}\sum_{i=0}^{m-1}\sum_{j=0}^{n-1}[P(i,j) - P'(i,j)]^2 \quad \ldots (7)$$

Peak Signal to Noise Ratio (PSNR)

PSNR is most simply defined by MSE. Eq. (8) gives the PSNR (in dB) definition.

$$PSNR = 10\ log_{10}\left(\frac{MAX_I^2}{MSE}\right) \quad \ldots (8)$$

where, MAX_I is the image's highest probable intensity of the image.

Structural Similarity Index (SSI)

SSI calculates how similar the two images are and its measurement between signals i and j is given by Eq. (9).

$$SSIM\ (i,j) = [l\ (i,j)]^{\propto}\ [c\ (i,j)]^{\beta}\ [\ s(i,j)]^{\gamma} \quad \ldots (9)$$

where, the terms $l\ (i,j)$, $c\ (i,j)$, and $s\ (i,j)$ denote luminousness, contrast, and structural comparisons correspondingly, and $\propto > 0, \beta > 0\ and\ \gamma > 0$ modifies the comparative weights of the three terms.

Image Enhancement Factor (IEF)

The Image Enhancement Factor (IEF) calculates the improvement in image quality following restoration. The IEF for a noise-free monochromatic image P of size m × n, its noisy estimate P', and the restored image P" can be represented as Eq. (10).

$$IEF = \left(\frac{\sum_i\sum_j(P'(i,j) - P(i,j)^2}{\sum_i\sum_j(P''(i,j) - P(i,j)^2}\right) \quad \ldots (10)$$

The restoration of the corrupted images is performed using CMF[6], CWMF[8], SM[10], BDND[21], FIDRM[25], and FBDA[26] and the proposed FDBF filtering methods. The restoration results of two test images for 30%, 60%, and 90% noise density levels are presented in this paper. The image quality metrics defined above are calculated on the given test MR Images for the different techniques and a comparative analysis is presented. The performance evaluation of the proposed method has been discussed in the context of restoration and detector performance compared with other existing methods.

Restoration Performance

The image details are retained in terms of the visible attributes of the restored images for CMF, CWMF, and SM, but couldn't succeed in removing noise completely at ND 50%. However, BDND, FIDRM, FBDA, and the FDBF methods remove noise completely at ND 50% without sacrificing the finer details. At ND > 60%, CMF, CWMF, and SM fail to remove noise and do not preserve image information whereas BDND and FIDRM are unable to eliminate noise while preserving image features. However, the restoration outcomes for FBDA and FBDF are comparable. Nevertheless, the suggested FDBF approach restores MR Images without blurring or losing image information, while FBDA produces blurring in the restored images at ND > 90%. The restoration outcomes for images 1 and 2 are given in Figs 2–4 and 5–7, respectively, at 30, 60, and 90% noise density.

Experimental results for image quality assessment measures as defined by Eqs 7–10 for test images 1 and 2 are summarised in Tables 1 & 2 respectively. It is apparent from the findings that the proposed FDBF surpasses the other filters concerning PSNR, MSE, SSIM, and the perceived quality of the image. FDBF and the other filtering methods like CMF, CWMF, SM, BDND FIDRM, and FBDA all perform identically with only a slight variation in image quality metrics at ND > 50%. The image quality criteria for ND > 50 deviate significantly from those for the proposed FDBF.

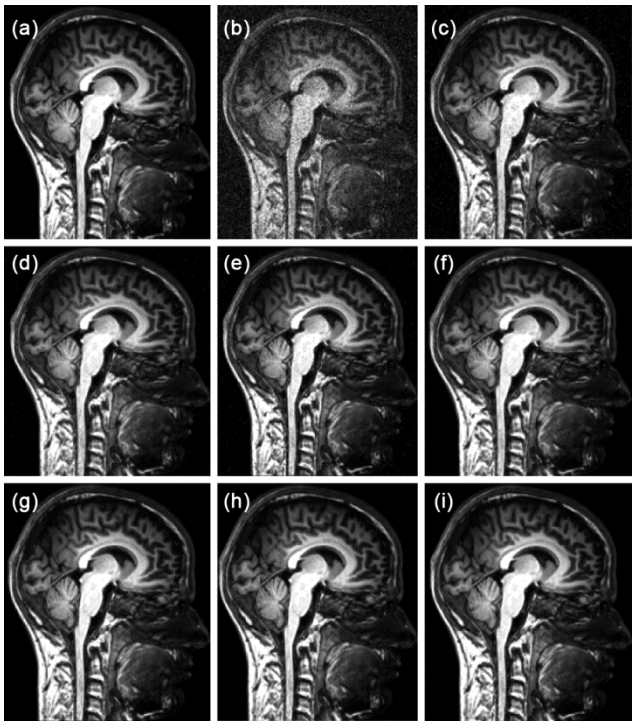

Fig. 2 — Restoration results at 30% ND: (a) test image 1, (b) noisy image, (c) CMF, (d) CWMF, (e) SM, (f) BDND, (g) FIDRM, (h) FBDA, (i) proposed FDBF

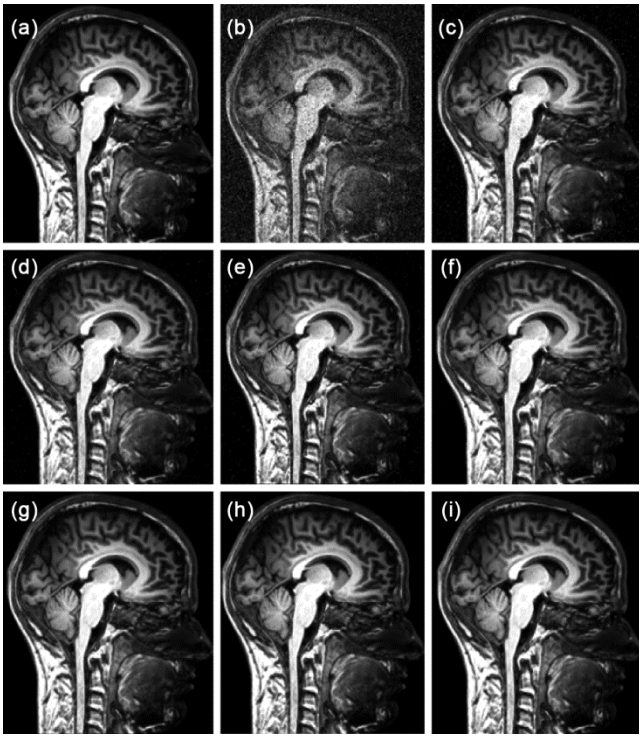

Fig. 3 — Restoration results at 30% ND: (a) test image 1, (b) noisy image, (c) CMF, (d) CWMF, (e) SM, (f) BDND, (g) FIDRM, (h) FBDA, (i) proposed FDBF (h) FBDA, (i) proposed FDBF

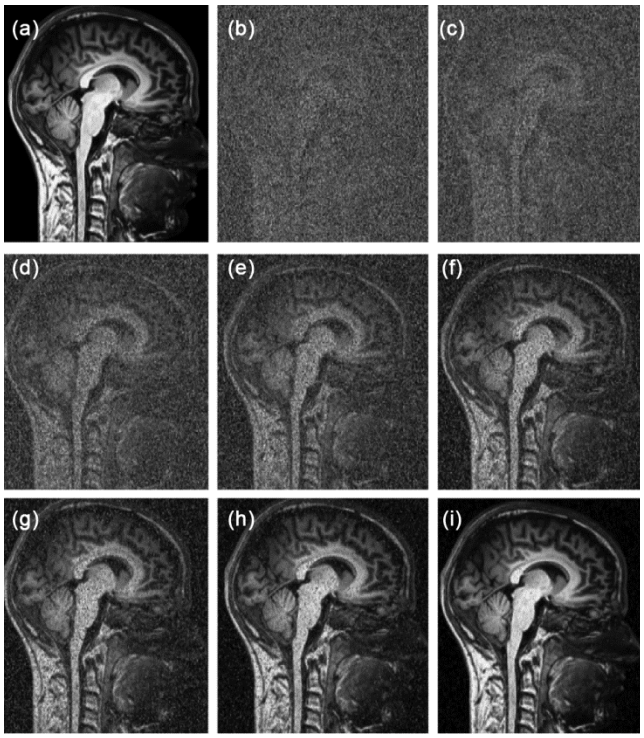

Fig. 4 — Restoration results at 90% ND: (a) test image 1, (b) noisy image, (c) CMF, (d) CWMF, (e) SM, (f) BDND, (g) FIDRM, (h) FBDA, (i) proposed FDBF

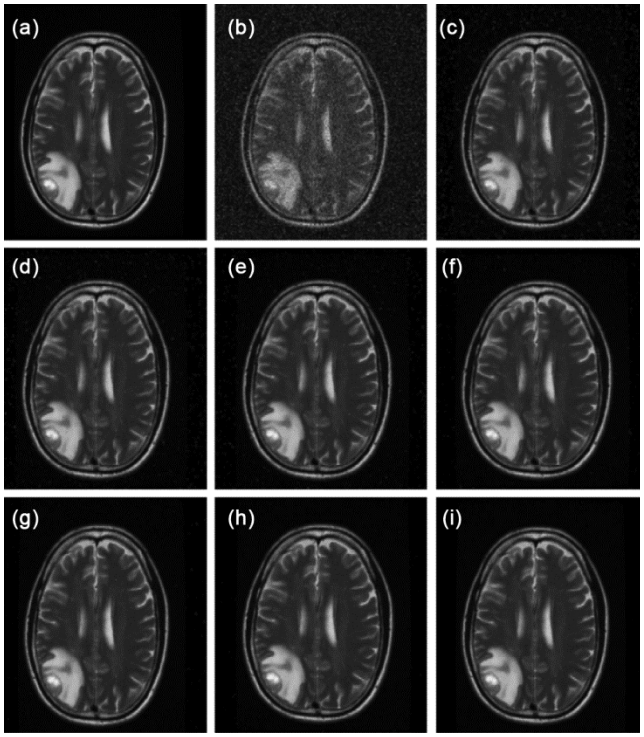

Fig. 5 — Restoration results at 30% ND: (a) test image 2, (b) noisy image, (c) CMF, (d) CWMF, (e) SM, (f) BDND, (g) FIDRM, (h) FBDA, (i) proposed FDBF

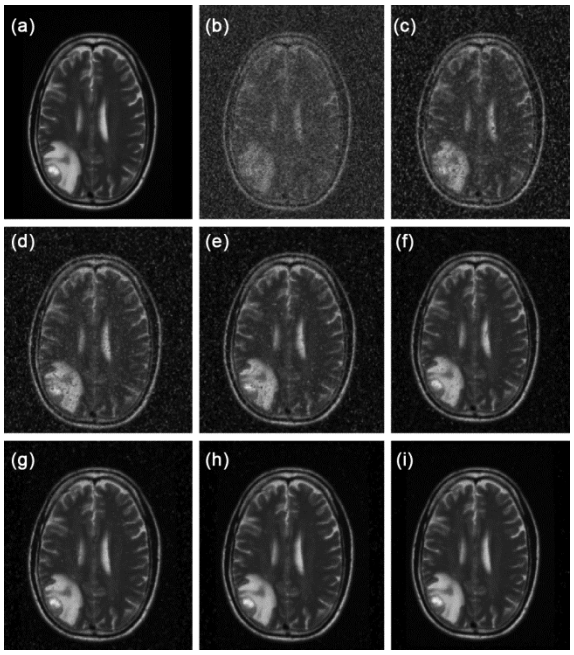

Fig. 6 — Restoration results at 60% ND: (a) test image 2, (b) noisy image, (c) CMF, (d) CWMF, (e) SM, (f) BDND, (g) FIDRM, (h) FBDA, (i) proposed FDBF

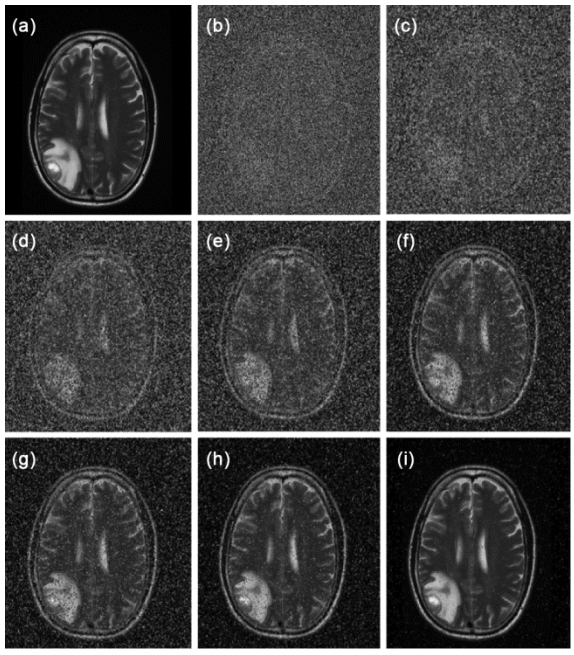

Fig. 7 — Restoration results at 90% ND: (a) test image 2, (b) noisy image, (c) CMF, (d) CWMF, (e) SM, (f) BDND, (g) FIDRM, (h) FBDA, (i) proposed FDBF

Table 1 — Comparative evaluation of different filters for the input test image 1 at varied noise densities

Methods									
PSNR (in dB)	10%	20%	30%	40%	50%	60%	70%	80%	90%
CMF	35.79	30.38	24.61	20.11	16.73	14.16	12.19	10.65	9.36
CWMF	35.67	32.14	27.79	23.62	20.21	16.14	14.19	12.16	10.51
SM	36.94	33.44	29.12	24.67	22.32	17.41	15.44	13.37	11.34
BDND	37.44	34.39	31.55	26.84	24.56	20.07	17.98	15.64	13.10
FIDRM	38.03	35.94	33.32	30.24	27.34	23.62	22.11	20.13	16.75
FBDA	38.35	36.85	35.03	32.63	30.35	27.40	25.70	23.56	20.16
FDBF	39.14	37.58	36.80	34.86	33.26	31.62	29.76	27.99	24.55
MSE									
CMF	0.0003	0.0009	0.0035	0.0097	0.0212	0.0384	0.0603	0.0861	0.1157
CWMF	0.0002	0.0006	0.0017	0.0043	0.0095	0.0243	0.0381	0.0607	0.0888
SM	0.0002	0.0005	0.0012	0.0034	0.0059	0.0181	0.0286	0.0460	0.0733
BDND	0.0002	0.0004	0.0007	0.0021	0.0035	0.0098	0.0159	0.0273	0.0489
FIDRM	0.0002	0.0003	0.0005	0.0009	0.0018	0.0043	0.0061	0.0097	0.0211
FBDA	0.0001	0.0002	0.0003	0.0005	0.0009	0.0018	0.0027	0.0044	0.0096
FDBF	0.0001	0.0002	0.0002	0.0003	0.0005	0.0007	0.0011	0.0016	0.0035
SSIM									
CMF	97.12	89.18	70.19	50.25	35.65	24.62	16.47	10.38	5.97
CWMF	97.64	92.76	82.28	65.80	50.85	33.28	24.76	16.36	9.57
SM	97.83	94.71	86.03	70.30	60.11	38.51	30.03	21.26	13.09
BDND	98.03	95.99	92.01	78.64	70.28	50.42	41.10	30.58	20.28
FIDRM	98.23	97.31	94.69	89.18	80.40	65.86	59.51	50.34	35.74
FBDA	98.33	97.79	96.59	93.79	89.23	80.72	74.81	65.64	50.82
FDBF	98.51	98.08	97.77	96.53	94.65	91.94	87.81	82.82	70.27
IEF									
CMF	44.32	33.59	17.69	8.18	4.78	3.17	2.35	1.88	1.58
CWMF	93.76	81.93	69.36	54.97	44.49	37.33	30.19	26.33	20.84
SM	137.04	125.02	106.59	97.83	85.04	73.34	67.87	54.80	42.07
BDND	172.67	162.99	149.30	125.53	107.48	92.23	85.86	74.01	62.69
FIDRM	191.97	178.42	162.62	142.84	127.42	114.96	101.52	88.35	79.81
FBDA	218.26	208.58	187.59	159.26	141.18	127.83	112.07	94.79	85.40
FDBF	239.10	227.90	207.84	194.12	176.50	153.24	140.90	130.70	117.35

Table 2 — Comparative evaluation of different filters for the input test image 2 at varied noise densities

Methods									
PSNR (in dB)	10%	20%	30%	40%	50%	60%	70%	80%	90%
CMF	36.87	29.72	23.65	18.83	15.38	12.9	10.97	9.1643	8.26
CWMF	37.56	32.17	27.17	22.37	18.96	14.89	12.85	11.02	9.16
SM	38.01	32.75	28.6	23.64	21	15.98	14.15	12.01	9.96
BDND	38.57	34.89	31.4	25.82	23.43	18.72	16.66	14.4	11.76
FIDRM	39.31	36.67	33.23	29.86	26.64	22.5	20.88	18.76	15.46
FBDA	39.93	37.92	35.51	32.55	29.97	27.02	24.63	22.43	18.94
FDBF	41	38.59	37.72	35.38	33.47	31.14	29.14	27.05	23.57
MSE									
CMF	0.0002	0.0011	0.0043	0.0131	0.029	0.0513	0.08	0.1212	0.1489
CWMF	0.0002	0.0006	0.0019	0.0058	0.0127	0.0324	0.0518	0.0791	0.1213
SM	0.0002	0.0005	0.0014	0.0043	0.0079	0.0252	0.0384	0.0629	0.1009
BDND	0.0001	0.0003	0.0007	0.0026	0.0045	0.0134	0.0216	0.0363	0.0667
FIDRM	0.0001	0.0002	0.0005	0.001	0.0022	0.0056	0.0082	0.0133	0.0284
FBDA	0.0001	0.0002	0.0003	0.0006	0.001	0.002	0.0034	0.0057	0.0127
FDBF	0.0001	0.0001	0.0002	0.0003	0.0004	0.0008	0.0012	0.002	0.0044
SSIM									
CMF	98.07	87.29	61.48	38.48	26.23	18.38	12.22	70.53	40.33
CWMF	98.39	92.43	77.25	55.36	38.68	24.01	18.46	12.22	7.54
SM	98.72	93.91	82.89	61.34	48.07	28.07	22.42	15.92	9.81
BDND	98.87	96.42	90.82	71.69	60.7	38.86	30.43	22.54	14.76
FIDRM	98.96	97.89	94.44	86.79	75.08	55.89	48.36	38.76	26.11
FBDA	99.07	98.55	97	93.19	87.11	77.49	67.03	55.79	38.77
FDBF	99.18	98.87	98.44	97.06	94.48	90.4	85.34	77.81	60.89
IEF									
CMF	60.53	43.35	16.36	7.21	4.07	2.74	2.03	1.55	1.41
CWMF	108.21	95.46	79.36	62.99	57.36	43.74	32.71	26.06	21.56
SM	149.49	136.66	107.41	96.25	90.31	76.47	63.35	52.4	41.74
BDND	171.02	163.46	147.89	123.39	115.54	97.01	85	73.49	62.29
FIDRM	213.31	201.06	174.18	145.58	126.97	113.32	100	87.03	74.12
FBDA	246.25	236.86	220.83	187.95	146.67	128.38	118.94	103.1	97.36
FDBF	278.68	269.19	256.2	239.96	217.77	194.48	179.95	158.28	146.02

Detection Performance

The restoration technique's effectiveness is mostly influenced by the noise detector's performance. As shown in Table 3, based on miss (undetected) and false (wrongly identified) detections, other noise detection schemes are contrasted with the proposed SFCM-based detector to assess its performance. When compared to noise-free pixels, the pixel intensities of noisy pixels for RVIN do not differ significantly. A decent noise detector should be able to recognize every noisy pixel with the least amount of false positives. A difference-based approach is used to calculate the rates of Falsely Detected (FD) and Miss-Detected (MD) pixel. The noise matrix is generated based on the estimation of differences between the original and noisy matrices. The increase in the miss detection rate will lead to blurring of the image, while the rise in the false detection rate will lead to image damage due to many residual noises.

Table 3 — Comparative analysis of miss and false detection rates at varied noise-density for the MR test image 1

Noise Density	30%		60%		90%	
Methods	MDR (%)	FDR (%)	MDR (%)	FDR (%)	MDR (%)	FDR (%)
SM	9.37	0.70	22.56	5.67	30.08	7.42
BDND	6.71	0.59	20.01	4.64	31.71	6.34
FIDRM	2.54	4.99	18.87	4.91	43.01	3.54
FBDA	5.31	0.19	17.24	2.13	28.67	4.13
FBDF	1.09	0.04	3.56	0.56	3.75	2.44

For the test, MR image 1 (672 × 634) the number of uncorrupted pixels classified as noisy (FD) and the percentage of unnoticed noisy pixels (MD) are determined for various noise detectors and are shown in Table 3. The findings demonstrate that, given a minimum MD and FD rates %, the proposed SFCM-based detector beats the other noise detectors.

Based on the restoration and detection findings, it can be concluded that the FDBF filter delivers notable improvements in comparison to the other filters. In our computing environment, we also determined the

algorithm execution time using a system with an Intel(R) Core (TM) i7-8700 CPU with 3.20 GHz, running RAM of 16.0 GB, and 64-bit Windows 10 Pro. It takes 0.46, 0.97, and 1.32 (in seconds) to fully restore an MR picture that has been contaminated by noise densities of 30, 60, and 90%.

Conclusions

A two-step FDBF is intended for the effective restoration of high-density RVIN-corrupted MR images. Instead of substituting the median value for the corrupted pixel, the suggested decision-based solution takes advantage of the spatial relationship between the neigh boring pixels to detect and restore the corrupted pixel. SFCM carries out impulse detection efficiently despite very high noise densities, while IBFE determines the restoration value of the corrupted pixels by taking neighbour pixel correlation into consideration leading to edge preservation. To achieve the finest possible restored image, the restoration process only needs to be repeated a few times. The proposed FDBF method's ability to preserve edges and finer image features even at high noise levels and cheap operating costs is confirmed by experimental results, making it a good choice for edge devices. The restoration time for an MR image corrupted with 90% noise density was found to be 1.32 seconds.

It has been observed that the pixels incorrectly identified or overlooked are primarily present in the image's contour and edge regions and are therefore considered to be noise. Both the detection and restoration processes are hampered by excessive noise in the detail regions restricting the performance of the study. For real-time applications, the detector performance and operational costs can be further improved to make it more suitable in the subsequent study.

References

1 Gerig G, Kubler O, Kikinis R & Jolesz F A, Nonlinear anisotropic filtering of MRI data, *IEEE Trans Med Imaging*, **11(2)** (1992) 221–232, DOI:10.1109/42.141646.

2 Saxena P & Kumar R S, An effective filter for noise removal in magnetic resonance images using multilevel fuzzy reasoning concept, *J Clin Eng*, **42(3)** (2017) 121–135, DOI: 10.1097/JCE.0000000000000224.

3 Lin P H, Chen B H, Cheng F C & Huang S C, A morphological mean filter for impulse noise removal, *J Display Technol*, **12(4)** (2016) 344–350, DOI:10.1109/JDT.2015.2487559.

4 Yeganli S F, Demirel H & Yu R, Noise removal from MR images via iterative regularization based on higher-order singular value decomposition, *Signal Image Video Process*, **11** (2017) 1477–1484, https://doi.org/10.1007/s11760-017-1110-y.

5 Gonzalez R C & Woods R E, *Digital Image Processing*, **3rd edn** (Prentice-Hall, Englewood Cliffs NJ) 2008.

6 Huang T, Yang G & Tang G, A fast two-dimensional median filtering algorithm, *IEEE Trans Signal Process*, **27(1)** (1979) 13–18, DOI: 10.1109/TASSP.1979.1163188.

7 Brownrigg D R, The weighted median filter, *Commun, ACM*, **27(8)** (1984) 807–818.

8 Ko S J & Lee Y H, Center weighted median filters and their applications to image enhancement, *IEEE Trans Circuits Syst*, **38(9)** (1991) 984–993, DOI: 10.1109/31.83870.

9 Hwang H & Haddad R A, Adaptive median filters: new algorithms and results, *IEEE Trans Image Process*, **4(4)** (1995) 499–502, DOI: 10.1109/83.370679.

10 Chen T, Ma K K & Chen L H, Tri-state median filter for image denoising, *IEEE Trans Image Process*, **8(12)** (1999) 1834–1838, DOI: 10.1109/83.806630

11 Zhang S & Karim M A, A new impulse detector for switching median filters, *IEEE Signal Process Lett*, **9(11)** (2002) 360–363, DOI:10.1109/LSP.2002.805310.

12 Sun T & Neuvo Y, Detail-preserving median based filters in image processing, *Pattern Recognit Lett*, **15(4)** (1994) 341–347, DOI:10.1016/0167-8655(94)90082-5.

13 Aizenberg I & Butakoff C, Effective impulse detector based on rank-order criteria, *IEEE Signal Process Lett*, **11(3)** (2004) 363–366, DOI: 10.1109/LSP.2003.822925.

14 Garnett R, Huegerich T, Chui C & He W, A universal noise removal algorithm with an impulse detector, *IEEE Trans Image Process*, **14(11)** (2005) 1747–1754, DOI:10.1109/TIP.2005.857261.

15 Zhou Y Y, Ye Z F & Huang J J, Improved decision-based detail-preserving variational method for removal of random-valued impulse noise, *IET Image Process*, **6(7)** (2012) 976–985, DOI:10.1049/iet-ipr.2011.0312.

16 Kayhan S K, An effective 2-stage method for removing impulse noise in images, *J Vis Commun Image Represent*, **25(2)** (2014) 478–486, DOI:10.1016/j.jvcir.2013.12.016.

17 Horng S J, Hsu L Y, Li T, Qiao S, Gong X, Chou H H & Khan M K, Using sorted switching median filter to remove high-density impulse noises, *J Vis Commun Image Represent*, **24(7)** (2013) 956–967, DOI:10.1016/j.jvcir.2013.06.012

18 Zhang J, An efficient median filter-based method for removing random-valued impulse noise, *Digit Signal Process*, **20(4)** (2010) 1010–1018, DOI: 10.1016/j.dsp.2009.11.003.

19 Abreu E, Lightstone M, Mitra S K & Arakawa K, A new efficient approach for the removal of impulse noise from highly corrupted images, *IEEE Trans Image Process*, **5(6)** (1996) 1012–1025, DOI:10.1109/83.503916.

20 Eng H L & Ma K K, Noise adaptive soft-switching median filter, *IEEE Trans Image Process*, **10(2)** (2001) 242–251, DOI:10.1109/83.902289.

21 Ng P E & Ma K K, A switching median filter with boundary discriminative noise detection for extremely corrupted images, *IEEE Trans Image Process*, **15(6)** (2006) 1506–1516, DOI: 10.1109/TIP.2005.871129.

22 Jafar I F, AlNa'mneh R A & Darabkh K A, Efficient improvements on the BDND filtering algorithm for the removal of high-density impulse noise, *IEEE Trans Image*

Process, **22(3)** (2012) 1223–1232, DOI:10.1109/TIP.2012.2228496.

23 Roy A, Chandra S & Rabidas R, Improved switching vector median filter for removal of impulse noise from color images, *Proc Adv Smart Commun Imag Syst: Lect Notes Electr Eng* (Springer Singapore) **721** (2020) 11–19, DOI:10.1007/978-981-15-9938-5_2.

24 Mélange T, Nachtegael M, Schulte S & Kerre E E, A fuzzy filter for the removal of random impulse noise in image sequences, *Image Vis Comput*, **29(6)** (2011) 407–419, DOI: https://doi.org/10.1016/j.imavis.2011.01.005.

25 Schulte S, Nachtegael M, De Witte V, Van der Weken D & Kerre E E, A fuzzy impulse noise detection and reduction method, *IEEE Trans Image Process*, **15(5)** (2006) 1153–1162, DOI:10.1109/TIP.2005.864179.

26 Nair M S & Raju G, A new fuzzy-based decision algorithm for high-density impulse noise removal, *Signal Image Video Process*, **6** (2012) 579–595, DOI:10.1007/s11760-010-0186-4.

27 Toprak A & Güler İ, Suppression of impulse noise in medical images with the use of a fuzzy adaptive median filter, *J Med Syst*, **30** (2006) 465–471, DOI: 10.1007/s10916-006-9031-2.

28 Schulte S, De Witte V, Nachtegael M, Van der Weken D & Kerre E E, Fuzzy two-step filter for impulse noise reduction from color images, *IEEE Trans Image Process*, **15(11)** (2006) 3567–3578, DOI: 10.1109/TIP.2006.877494.

29 Nadeem M, Hussain A, Munir A, Habib M & Naseem M T, Removal of random valued impulse noise from grayscale images using quadrant based spatially adaptive fuzzy filter, *Signal Process*, **169** (2020) 107403, DOI: 10.1016/j.sigpro.2019.107403.

30 Azhar M, Dawood H, Dawood, H, Choudhary G I, Bashir A K & Chaudhary S H, Detail-preserving switching algorithm for the removal of random-valued impulse noise, *J Ambient Intell Humaniz Comput*, **10(10)** (2019) 3925–3945, DOI: 10.1007/s12652-018-1153-0.

31 Turkmen I, A new method to remove random-valued impulse noise in images, *Int J Electron Commun*, **67(9)** (2013) 771–779, DOI: https://doi.org/10.1016/j.aeue.2013.03.006.

32 Thakur R S, Chatterjee S, Yadav R N & Gupta L, Image de-noising with machine learning: A review, *IEEE Access*, **9** (2021) 93338–93363, DOI: 10.1109/ACCESS.2021.3092425.

33 Xing Y, Xu J, Tan J, Li D & Zha W, Deep CNN for removal of salt and pepper noise, *IET Image Process*, **13(9)** (2019) 1550–1560, DOI:10.1049/iet-ipr.2018.6004.

34 Fu B, Zhao X, Li Y, Wang X & Ren Y, A convolutional neural networks denoising approach for salt and pepper noise, *Multimed Tools Appl*, **78** (2019) 30707–30721, DOI:10.1007/s11042-018-6521-4.

35 Sadrizadeh S, Otroshi-Shahreza H & Marvasti F, Impulsive noise removal via a blind CNN enhanced by iterative post-processing, *Signal Process*, **192** (2022) 108378, DOI:10.1016/j.sigpro.2021.108378.

36 Cai W, Chen S & Zhang D, Fast and robust fuzzy c-means clustering algorithms incorporating local information for image segmentation, *Pattern Recognit*, **40(3)** (2007) 825–838, DOI: 10.1016/j.patcog.2006.07.011.

37 Choudhry M S & Kapoor R, Performance analysis of fuzzy C-means clustering methods for MRI image segmentation, *Procedia Comput Sci*, **89** (2016) 749–758, DOI: 10.1016/j.procs.2016.06.052

38 Wang Zhou, Alan C Bovik, Hamid R Sheikh & Eero P Simoncelli, Image quality assessment: from error visibility to structural similarity, *IEEE Trans Image Process*, **13(4)** (2004) 600–612, DOI: 10.1109/TIP.2003.819861